IJMMM International Journal of Minerals, Metallurgy and Materials 矿物冶金与材料学报（英文版）

Mixed ion and electron transport theory and application in solid oxide conductors

Kevin Huang

Cite this article as:
Kevin Huang, Mixed ion and electron transport theory and application in solid oxide conductors, *Int. J. Miner. Metall. Mater.*, 29(2022), No. 4, pp. 870-875. https://doi.org/10.1007/s12613-021-2401-4

View the article online at SpringerLink or IJMMM Webpage.

IJMMM WeChat

QQ author group

International Journal of Minerals, Metallurgy and Materials
Volume 29, Number 4, April 2022, Page 870
https://doi.org/10.1007/s12613-021-2401-4

Invited Review

Mixed ion and electron transport theory and application in solid oxide conductors

Kevin Huang✉

Department of Mechanical engineering, University of South Carolina, Columbia, SC 292201, USA
(Received: 26 October 2021; revised: 30 November 2021; accepted: 20 December 2021)

Abstract: Mixed ions and electron conductors (MIECs) are an important family of electrocatalysts for electrochemical devices, such as reversible solid oxide cells, rechargeable metal–air batteries, and oxygen transport membranes. Concurrent ionic and electronic transports in these materials play a key role in electrocatalytic activity. An in-depth fundamental understanding of the transport phenomena is critically needed to develop better MIECs. In this brief review, we introduced generic ionic and electronic transport theory based on irreversible thermodynamics and applied it to practical oxide-based materials with oxygen vacancies and electrons/holes as the predominant defects. Two oxide systems, namely CeO_2-based and $LaCrO_3$-based materials, are selected as case studies to illustrate the utility of the transport theory in predicting oxygen partial pressure distribution across MIECs, electrochemical electronic/ionic leakage currents, and the effects of external load current on the leakage currents.

Keywords: irreversible thermodynamics; diffusivity; charge neutrality; electrochemical potential; electrostatic potential

1. Introduction

Mixed ions and electron conductors (MIECs) have a wide range of applications in electrochemical devices, such as reversible solid oxide cells (RSOCs) [1], rechargeable metal–air batteries (RMABs) [2], and oxygen transport membranes (OTMs) [3]. Their high electrocatalytic activity is considered to arise from the enhanced partial ionic conductivity (σ_i) by the overwhelming electronic conductivity via the "drag-pull" mechanism to satisfy the local charge-neutrality requirement [4]. However, ionic transport should be minimized for applications that use conducting ceramics as an electronic conductor. A good example is the doped $LaCrO_3$ as a ceramic interconnect (IC) material for solid oxide fuel cells (SOFCs). Since one important functionality of ICs is to pass electrons from cathode to anode (or vice versa), any oxide-ion conductivity in the IC would induce a net oxygen flux flow from high partial pressure of oxygen (P_{O_2}) like air to low P_{O_2} such as fuels. Such oxygen leakage results in additional oxidation of fuels without producing electricity to the external circuit, lowering the electrical efficiency. Conversely, minor electronic conduction could be detrimental to MIEC with ions as a major charge carrier and electrons as a minor charge carrier. Doped CeO_2 is a good example of an electrolyte for SOFCs. In reducing atmospheres, the reducibility of Ce^{4+} to Ce^{3+} would cause n-type electronic conductivity, resulting in an electronic leakage current, lowering the open-circuit voltage (OCV) and electrical efficiency of SOFCs.

From an engineering perspective, quantification of these leakage currents in MIECs is important for the design and healthy operation of electrochemical devices using them. Unfortunately, there is scarce literature dealing with the leakage phenomenon and quantifying the leakage current.

In this short review, we aim to bridge this gap by reviewing classic phenomenological transport theory involving mixed ions and electrons. Further, we applied the theory to two representative MIECs, viz., doped CeO_2 and doped $LaCrO_3$, demonstrating calculations of P_{O_2} distribution across MIECs and leakage currents in SOFCs under both OCV and loading conditions.

2. General bulk transport theory

The theory of bulk transport of charged particles in solids is generally described by the principles of irreversible thermodynamics [4–7]. If a conducting solid contains species $\boldsymbol{k}$ with charge z_k and conductivity σ_k, its one-dimensional flux density j_k is proportional to the gradient of η_k across the thickness. Hence,

$$j_k = -\frac{\sigma_k}{z_k^2 F^2}\nabla\eta_k \tag{1}$$

where η_k is the electrochemical potential of species $\boldsymbol{k}$, and $\eta_k = \mu_k + z_k F\phi$, wherein μ_k is the chemical potential of species $\boldsymbol{k}$, ϕ is the electrostatic potential, and F is Faraday's constant. From Faraday's law, the corresponding current density i_k is derived as follows:

✉ Corresponding author: Kevin Huang E-mail: huang46@cec.sc.edu

$$i_k = z_k F j_k = -\frac{\sigma_k}{z_k F}\nabla\eta_k \tag{2}$$

Notably, the assumptions under which the above basic flux equations are valid [4] include (1) isotropic diffusion, (2) the chemical potential gradient $\Delta\mu$ across the solid is smaller than RT (R and T represent gas constant and absolute temperature, respectively) so that a linear relationship exists between j_k and $\nabla\phi$, (3) the Onsager cross-coefficients are ignored, (4) local equilibria are established between solid and gas phases, and (5) all fluxes, forces, and gradients are along one given diffusion direction (x-direction). Therefore, the concentrations and fluxes have the same value at any position on a given plane normal to this direction. Eqs. (1) and (2) are the foundations for evaluating the transport properties of charge carriers in solids.

For a solid with multiple charge carriers, the net current density of all charge carriers must equal zero in the absence of external current due to the requirement of charge neutrality [4]. Hence,

$$\sum_k i_k = 0 \text{ or } \sum_k z_k j_k = 0 \tag{3}$$

When applying Eq. (3) to multiple charge carriers in motion, it is often termed as "quasi-neutrality" to capture the slight concentration mis-adjustment induced by the electrostatic force [4]. The "quasi-neutrality" holds for the sample with a dimension greater than the Debye length. The "quasi-neutrality" rule is then given by Ref. [4] as follows:

$$\sum_k z_k \nabla c_k = 0 \tag{4}$$

where ∇c_k is the concentration c_k gradient of species $\boldsymbol{k}$. Using the transport number $t_k = \sigma_k/\sigma$, where $\sigma = \sum_k \sigma_k$ is the total electrical conductivity of the charge carrier $\boldsymbol{k}$, and combining Eqs. (1)–(4), we get

$$\sum_k \frac{t_k}{z_k}\nabla\eta_k = 0 \tag{5}$$

The electrical conductivity σ_k is closely related to the diffusivity D_k^σ defined in the Nernst–Einstein equation:

$$\frac{\sigma_k}{z_k^2 F^2} = \frac{c_k D_k^\sigma}{RT} \tag{6}$$

It is evident that if σ_k and c_k are known, Eq. (6) can be used to determine D_k^σ. Therefore, D_k^σ in Eq. (6) is often referred to as the conductivity-related diffusivity [8].

Several other types of commonly used diffusivities are defined based on the methods deriving them [8]. For example, tracer diffusivity (D^*) is often obtained with isotope exchange coupled with secondary ion mass spectroscopy, and chemical diffusivity ($\tilde{D}$) and ambipolar diffusivity (D_a) are derived from electrical conductivity relaxation or chemical cells methods.

It is cautioned that different diffusivity terms are used for specific scenarios. The tracer diffusivity D_k^* relates to the conductivity D_k^σ by the Haven ratio H_R. Accordingly,

$$D_k^* = H_R D_k^\sigma \tag{7}$$

where H_R correlates the migration of lattice atoms in successful jumps with that of ionic defects in crystalline ionic conductors. In many cases, H_R equals the correlation factor f [9].

Since many MIECs are operated under a chemical potential gradient, measuring transport properties under real operating conditions is more meaningful. Therefore, chemical diffusivity ($\tilde{D}$) and ambipolar diffusivity (D_a) are more useful terms for describing the transport properties of MIECs. In theory, $\tilde{D}$ is related to component diffusivity of charge carrier $\boldsymbol{k}$, D_k. Hence, by Ref. [4],

$$\tilde{D} = (D_k t_{e'})\frac{\nabla \ln a_{k^*}}{\nabla \ln c_{k^*}} = (D_k t_{e'})\xi \tag{8}$$

where $\boldsymbol{k}^*$ represents the neutral species of $\boldsymbol{k}$ charge carrier; a_{k^*} and c_{k^*} are activity and concentration of neutral species $\boldsymbol{k}^*$; $t_{e'}$ is the electronic transport number; ξ is "thermodynamic factor" or "enhancement factor".

The ambipolar diffusivity D_a is another term to describe a simultaneous diffusion of ions and electrons. It relates to D_k and $D_{e'}$ (diffusivity of electrons) by Ref. [4] as follows:

$$D_a = t_{e'} D_k + t_k D_{e'} \tag{9}$$

which can further be simplified into the following for $D_{e'} >> D_k$ and $t_{e'} \approx 1$:

$$D_a \approx t_k D_{e'} \tag{10}$$

It is not difficult to find that $D_a > D_k$ and D_a is usually large [4].

3. Application of transport theory to solid oxide electrolytes

3.1. Distribution of partial pressure of oxygen across a CeO_2-based electrolyte

The stead-state P_{O_2} (or oxygen activity) profile across an electrolyte membrane with minor electronic conduction can be calculated using the above transport equations. Choudhury and Patterson [10] and Riess [11] were the first to calculate the oxygen profile across the electrolyte with minor electronic conduction. The calculations assume that oxygen vacancy $V_O^{\bullet\bullet}$ is the major ionic charge carrier and electron e′ is the minor charge carrier in electrolytes. The electrolyte of choice is any CeO_2-based material. The current densities (or flux densities) for each charge carrier in the bulk and external circuit are given by

$$i_{V_O^{\bullet\bullet}} = -\frac{\sigma_{V_O^{\bullet\bullet}}}{2F}\nabla\eta_{V_O^{\bullet\bullet}} \tag{11}$$

$$i_{e'} = \frac{\sigma_{e'}}{F}\nabla\eta_{e'} \tag{12}$$

$$i_L = \frac{\sigma_L}{F}\nabla\eta_{e'} \tag{13}$$

where i_L and σ_L represent load-current density and apparent electronic conductivity, respectively. From the charge-neutrality rule, we derive

$$i_{V_O^{\bullet\bullet}} + i_{e'} + i_L = 0 \tag{14}$$

Combining Eqs. (11)–(13) into Eq. (14) and solving for $\nabla\eta_{e'}$, we yield

$$\nabla\eta_{e'} = \frac{1}{2}\times\frac{\sigma_{V_O^{\bullet\bullet}}}{\sigma_{e'}+\sigma_L}\nabla\eta_{V_O^{\bullet\bullet}} \tag{15}$$

We considered that a local chemical equilibrium of $\frac{1}{2}O_2 + V_O^{\bullet\bullet} + 2e' = O_O^{\times}$ was established between the charged defects at the electrolyte surface, where $V_O^{\bullet\bullet}$ and $O_O^{\times}$ represent oxygen vacancy and oxygen lattice, respectively, according to the Kröger–Vink notation. The gradient of the chemical or electrochemical potential of each species holds the following relation:

$$\frac{1}{2}\nabla\mu_{O_2} + \nabla\eta_{V_O^{\bullet\bullet}} + 2\nabla\eta_{e'} = 0 \tag{16}$$

where the chemical potential gradient of neutral lattice oxygen $O_O^{\times}$ is zero, meaning that its concentration is constant across the electrolyte.

Substituting Eq. (16) into Eq. (15) yields

$$\nabla\eta_{e'} = -\frac{1}{4}\times\frac{\sigma_{V_O^{\bullet\bullet}}}{\sigma_{V_O^{\bullet\bullet}}+\sigma_{e'}+\sigma_L}\nabla\mu_{O_2} \tag{17}$$

Substituting Eq. (17) into Eqs. (11)–(13) leads to

$$i_{V_O^{\bullet\bullet}} = \frac{1}{4F}\times\frac{\sigma_{V_O^{\bullet\bullet}}(\sigma_{e'}+\sigma_L)}{\sigma_{V_O^{\bullet\bullet}}+\sigma_{e'}+\sigma_L}\nabla\mu_{O_2} \tag{18}$$

$$i_{e'} = -\frac{1}{4F}\times\frac{\sigma_{V_O^{\bullet\bullet}}\sigma_{e'}}{\sigma_{V_O^{\bullet\bullet}}+\sigma_{e'}+\sigma_L}\nabla\mu_{O_2} \tag{19}$$

$$i_L = -\frac{1}{4F}\times\frac{\sigma_{V_O^{\bullet\bullet}}\sigma_L}{\sigma_{V_O^{\bullet\bullet}}+\sigma_{e'}+\sigma_L}\nabla\mu_{O_2} \tag{20}$$

For an open-circuit condition, $i_{V_O^{\bullet\bullet}} = -i_{e'}$, and the following relationship can be derived as:

$$i_{V_O^{\bullet\bullet}}\mathrm{d}x = \frac{RT}{4F}\times\frac{\sigma_{V_O^{\bullet\bullet}}(\sigma_{e'}+\sigma_L)}{\sigma_{V_O^{\bullet\bullet}}+\sigma_{e'}+\sigma_L}\mathrm{d}(\ln Po_2) \tag{21}$$

Integrating Eq. (21) from 0 to x on the left-hand side and from $P_{O_2}(0)$ to $P_{O_2}(x)$ on the right-hand side, as shown in Fig. 1, the accumulative current density $i_{V_O^{\bullet\bullet}}(x)$ becomes

$$xi_{V_O^{\bullet\bullet}}(x) = \frac{RT}{4F}\int_{\ln Po_2(0)}^{\ln Po_2(x)}\frac{\sigma_{V_O^{\bullet\bullet}}(\sigma_{e'}+\sigma_L)}{\sigma_{V_O^{\bullet\bullet}}+\sigma_{e'}+\sigma_L}\mathrm{d}(\ln Po_2) \tag{22}$$

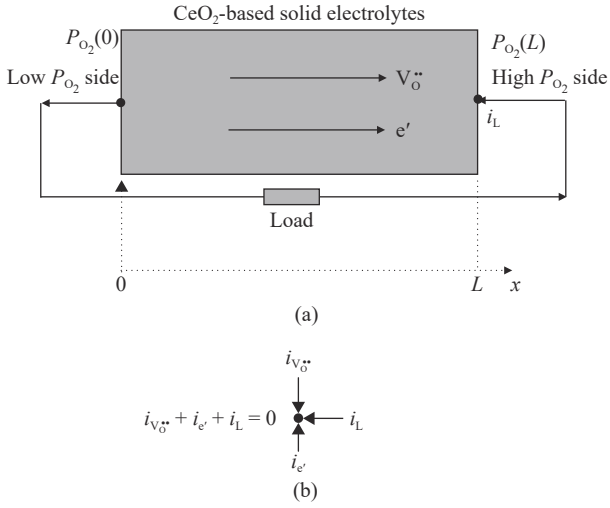

Fig. 1. (a) Illustration of transport of oxygen vacancies and electrons in CeO_2-based electrolytes; (b) charge-neutrality diagram.

At $x = L$, $i_{V_O^{\bullet\bullet}}(L)$ is given by

$$Li_{V_O^{\bullet\bullet}}(L) = \frac{RT}{4F}\int_{\ln Po_2(0)}^{\ln Po_2(L)}\frac{\sigma_{V_O^{\bullet\bullet}}(\sigma_{e'}+\sigma_L)}{\sigma_{V_O^{\bullet\bullet}}+\sigma_{e'}+\sigma_L}\mathrm{d}(\ln Po_2) \tag{23}$$

As $i_{V_O^{\bullet\bullet}}(x) = i_{V_O^{\bullet\bullet}}(L)$ at the steady state, the following relationship holds:

$$\frac{x}{L} = \frac{\int_{\ln Po_2(0)}^{\ln Po_2(x)}\frac{\sigma_{V_O^{\bullet\bullet}}(\sigma_{e'}+\sigma_L)}{\sigma_{V_O^{\bullet\bullet}}+\sigma_{e'}+\sigma_L}\mathrm{d}(\ln Po_2)}{\int_{\ln Po_2(0)}^{\ln Po_2(L)}\frac{\sigma_{V_O^{\bullet\bullet}}(\sigma_{e'}+\sigma_L)}{\sigma_{V_O^{\bullet\bullet}}+\sigma_{e'}+\sigma_L}\mathrm{d}(\ln Po_2)} \tag{24}$$

Notably, $\sigma_{V_O^{\bullet\bullet}}$ is independent of P_{O_2} for the electrolyte but $\sigma_{e'}$ varies with P_{O_2}, particularly in the low P_{O_2} range as $\sigma_{e'} = \sigma_{e'}^{o} Po_2^{-0.25}$ [12], where $\sigma_{e'}^{o}$ denotes electronic conductivity at P_{O_2} =1 atm (1.01×10^5 Pa). Substituting this relation into Eq. (24) gives the following:

$$\frac{x}{L} = \frac{\ln\left(\frac{\sigma_{V_O^{\bullet\bullet}}+\sigma_{e'}^{o}Po_2(x)^{-0.25}+\sigma_L}{\sigma_{V_O^{\bullet\bullet}}+\sigma_{e'}^{o}Po_2(0)^{-0.25}+\sigma_L}\right)+\ln\left(\frac{\sigma_{e'}^{o}+(\sigma_{V_O^{\bullet\bullet}}+\sigma_L)Po_2(x)^{0.25}}{\sigma_{e'}^{o}+(\sigma_{V_O^{\bullet\bullet}}+\sigma_L)Po_2(0)^{0.25}}\right)}{\ln\left(\frac{\sigma_{V_O^{\bullet\bullet}}+\sigma_{e'}^{o}Po_2(L)^{-0.25}+\sigma_L}{\sigma_{V_O^{\bullet\bullet}}+\sigma_{e'}^{o}Po_2(0)^{-0.25}+\sigma_L}\right)+\ln\left(\frac{\sigma_{e'}^{o}+(\sigma_{V_O^{\bullet\bullet}}+\sigma_L)Po_2(L)^{0.25}}{\sigma_{e'}^{o}+(\sigma_{V_O^{\bullet\bullet}}+\sigma_L)Po_2(0)^{0.25}}\right)} \tag{25}$$

With Eq. (25), P_{O_2} as a function of x/L across the electrolyte can be calculated, provided that $\sigma_{V_O^{\bullet\bullet}}$, $\sigma_{e'}^{o}$, and σ_L are known. For CeO_2-based electrolytes, these values have been compiled by Steele [13] for $Ce_{0.9}Gd_{0.1}O_{1.95}$ (GDC10) as follows:

$$\sigma_{V_O^{\bullet\bullet}}T = 1.09\times10^5\exp\left(-\frac{0.64\ \mathrm{eV}}{kT}\right)\quad(\mathrm{SK/cm}),(T>673\ \mathrm{K}) \tag{26}$$

$$\sigma_{V_O^{\bullet\bullet}}T = 1.00\times10^6\exp\left(-\frac{0.77\ \mathrm{eV}}{kT}\right)\quad(\mathrm{SK/cm}),(T<673\ \mathrm{K}) \tag{27}$$

$$\lg p_{e'} = -\frac{36970}{T}+18.00\qquad(\mathrm{atm}) \tag{28}$$

$$\sigma_{e'}T = 3.456\times10^9\exp\left(-\frac{2.475\ \mathrm{eV}}{kT}\right)Po_2^{-0.25}\qquad(\mathrm{SK/cm}) \tag{29}$$

where $p_{e'}$ is the specific partial pressure of oxygen at which $\sigma_{V_O^{\bullet\bullet}}=\sigma_{e'}$; k is the Boltzmann constant. Fig. 2 shows the calculated P_{O_2} profiles using Eq. (25) along with the parameters in

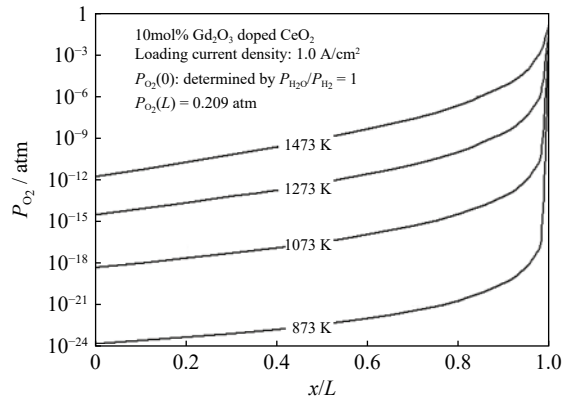

Fig. 2. Transmembrane P_{O_2} profiles in CeO_2-based electrolytes.

Eqs. (26)–(29) under different conditions. The transmembrane P_{O_2} profile is dominated by the low P_{O_2}, indicating the significant influence from electronic conduction, which has also been confirmed by the experiment [12].

3.2. Electron-induced leakage current density

Integrating Eq. (19) over the electrolyte thickness L and assuming $\sigma_{e'} = \sigma^{o}_{e'} Po_2^{-0.25}$ yields the following expression:

$$i_{e'} = \frac{RT\sigma_{V_O^{\bullet\bullet}}}{FL}\ln\left(\frac{\sigma_{V_O^{\bullet\bullet}} + \sigma^{o}_{e'} Po_2(L)^{-0.25} + \sigma_L}{\sigma_{V_O^{\bullet\bullet}} + \sigma^{o}_{e'} Po_2(0)^{-0.25} + \sigma_L}\right) \tag{30}$$

Similarly, the ionic current density $i_{V_O^{\bullet\bullet}}$ can be obtained by integrating Eq. (18) as:

$$i_{V_O^{\bullet\bullet}} = -\frac{RT\sigma_{V_O^{\bullet\bullet}}}{FL}\ln\left(\frac{\sigma_{V_O^{\bullet\bullet}} + \sigma^{o}_{e'} Po_2(L)^{-0.25} + \sigma_L}{\sigma_{V_O^{\bullet\bullet}} + \sigma^{o}_{e'} Po_2(0)^{-0.25} + \sigma_L}\right) - \frac{RT\sigma_{V_O^{\bullet\bullet}}\sigma_L}{FL(\sigma_{V_O^{\bullet\bullet}} + \sigma_L)}\ln\left(\frac{\sigma^{o}_{e'} + (\sigma_{V_O^{\bullet\bullet}} + \sigma_L) Po_2(L)^{0.25}}{\sigma^{o}_{e'} + (\sigma_{V_O^{\bullet\bullet}} + \sigma_L) Po_2(0)^{0.25}}\right) \tag{31}$$

As the interfacial $P_{O_2}(0)$ and $P_{O_2}(L)$ vary with load current i_L due to current-dependent electrode polarization, they must be solved first. Hence, the following boundary conditions for $i_{V_O^{\bullet\bullet}}$ are true for electrolyte, cathode, and anode layers under the stead-state as follows:

$$i_{V_O^{\bullet\bullet}}(\text{in electrolyte}) = i_{V_O^{\bullet\bullet}}(\text{in cathode}) = i_{V_O^{\bullet\bullet}}(\text{in anode}) \tag{32}$$

Assuming linear polarizations in the cathode and anode layers as

$$i_{V_O^{\bullet\bullet}}(\text{in cathode}) = \frac{RT}{4F}\times\frac{1}{R_c}\times\ln\frac{Po_2(\text{air})}{Po_2(L)} \tag{33}$$

$$i_{V_O^{\bullet\bullet}}(\text{in anode}) = \frac{RT}{4F}\times\frac{1}{R_a}\times\ln\frac{Po_2(0)}{Po_2(\text{fuel})} \tag{34}$$

where R_c and R_a are area specific resistances (ASRs) of the cathode and anode, respectively; P_{O_2}(air) and P_{O_2}(fuel) are the partial pressures of oxygen in bulk air and bulk fuel, respectively; $P_{O_2}(L)$ and $P_{O_2}(0)$ are the partial pressures of oxygen at the interfaces of electrolyte/cathode and electrolyte/anode, respectively.

Combining Eqs. (30)–(34) with the charge neutrality Eq. (14), $P_{O_2}(0)$ and $P_{O_2}(L)$ can be solved under different i_L, as shown in Fig. 3. The value of $P_{O_2}(0)$ nears that of $P_{O_2}(L)$ as i_L increases. Using the interfacial P_{O_2} in Fig. 3, $i_{e'}$ vs. i_L is further calculated and plotted in Fig. 4, where $i_{e'}$ decreases with i_L but increases with T, implying that the highest electronic leakage current density occurs under the open-circuit condition. Therefore, for CeO_2-based SOFCs, the leakage issue could be suppressed under loading operation, and its impact on electrical efficiency occurs in the low current density range where the electrical efficiency is supposed to be higher.

4. Application to interconnect

4.1. Distribution of partial pressure of oxygen in Ca-doped $LaCrO_3$ membrane

As another example, the above transport theory was used to evaluate the mixed ion and electron transport in an electron-dominated material Ca-doped $LaCrO_3$.

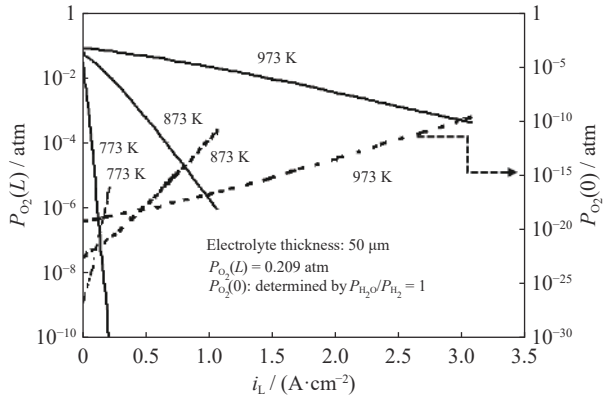

Fig. 3. Interfacial P_{O_2} vs. load-current density and temperatures. Solid lines: $P_{O_2}(L)$; dashed lines: $P_{O_2}(0)$. Anode ASR: R_a (Ω·cm^2) = 1.3 × 10^{-5}exp(9261/T); cathode ASR: R_c (Ω·cm^2) = 2.5 × 10^{-8}exp(13952/T) after Ref. [14].

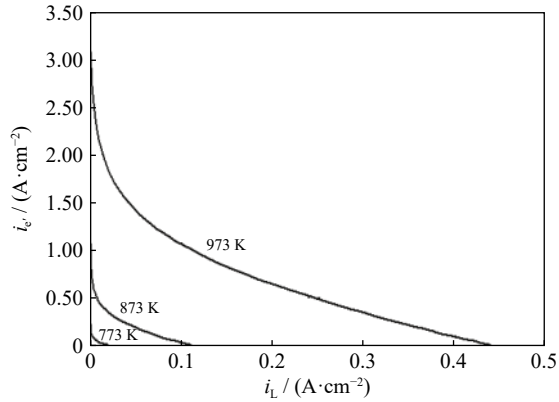

Fig. 4. Electronic leakage current density vs. load-current density of a CeO_2-based electrolyte.

The Ca-doped $LaCrO_3$ (LCC) contains predominant defect species Ca_{La}', $h^{\bullet}$ (electron holes), and oxygen vacancies $V_O^{\bullet\bullet}$. Its electrical conduction is dominated by localized small-polarons on the Cr-sites [15]. Therefore, $h^{\bullet}$ is equivalent to $Cr_{Cr}^{\bullet}$ (Cr^{4+}); thereby, $h^{\bullet}$ and $Cr_{Cr}^{\bullet}$ can be interchanged. The oxygen-LCC chemical equilibrium is established via

$$\frac{1}{2}O_2 + V_O^{\bullet\bullet} + 2Cr_{Cr}^{\times} = 2Cr_{Cr}^{\bullet} + O_O^{\times} \tag{35}$$

where $Cr_{Cr}^{\times}$ denotes regular neutral Cr lattice. Fig. 5 depicts a schematic illustration of the transport of charged species in LCC, considering $V_O^{\bullet\bullet}$ and $h^{\bullet}$.

From the basic current density equation (Eq. (2)), the current density of electron holes becomes

$$i_{h^{\bullet}} = -\frac{\sigma_{h^{\bullet}}}{F}\nabla\eta_{h^{\bullet}} \tag{36}$$

Given the local chemical equilibrium between $V_O^{\bullet\bullet}$ and $h^{\bullet}$, as shown in Eq. (35), the following relationships hold:

$$\begin{cases} \frac{1}{2}\nabla\mu_{O_2} + \nabla\mu_{V_O^{\bullet\bullet}} = 2\nabla\mu_{h^{\bullet}} \\ \nabla\mu_{e'} + \nabla\mu_{h^{\bullet}} = 0 \\ \nabla\eta_{e'} + \nabla\eta_{h^{\bullet}} = 0 \end{cases} \tag{37}$$

Combining the above equations leads to the one-dimensional distributions of ionic current density $i_{V_O^{\bullet\bullet}}$ and electron-hole current density $i_{h^{\bullet}}$,

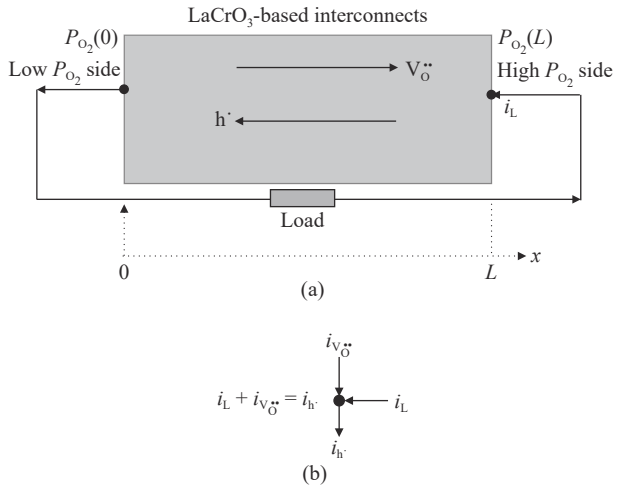

Fig. 5. (a) Illustration of charged species transport in a $LaCrO_3$-based interconnect; (b) charge-neutrality diagram.

$$i_{V_O^{\bullet\bullet}} = \frac{RT}{4F} \times \frac{\sigma_{V_O^{\bullet\bullet}} \times (\sigma_{h^\bullet} - \sigma_L)}{\sigma_{h^\bullet} - \sigma_{V_O^{\bullet\bullet}} - \sigma_L} \times \frac{\mathrm{d}(\ln Po_2)}{\mathrm{d}x} \tag{38}$$

$$i_{h^\bullet} = \frac{RT}{4F} \times \frac{\sigma_{V_O^{\bullet\bullet}} \times \sigma_{h^\bullet}}{\sigma_{h^\bullet} - \sigma_{V_O^{\bullet\bullet}} - \sigma_L} \times \frac{\mathrm{d}(\ln Po_2)}{\mathrm{d}x} \tag{39}$$

under the OCV condition $i_{V_O^{\bullet\bullet}}=i_{h^\bullet}$. Notably, different from oxide-ion conductors, both $\sigma_{V_O^{\bullet\bullet}}$ and $\sigma_{h^\bullet}$ in LCC vary with P_{O_2}.

According to Eq. (6), $\sigma_{V_O^{\bullet\bullet}}$ can be further expressed as follows:

$$\sigma_{V_O^{\bullet\bullet}} = \frac{4F^2 \times [V_O^{\bullet\bullet}] \times D_{V_O^{\bullet\bullet}}}{RT} \tag{40}$$

where $D_{V_O^{\bullet\bullet}}$ denotes the diffusivity of oxygen vacancies. Letting the concentration of $V_O^{\bullet\bullet}$ equal oxygen stoichiometry δ, $[V_O^{\bullet\bullet}] = \delta$, and considering the "quasi-neutrality" condition $p + 2\delta = y$, where p and y represent hole and dopant concentrations, respectively, the following relationship can be derived,

$$K = \frac{p^2 \times (6 - y + p)}{(1-p)^2 \times (y-p) \times P_{O_2}^{1/2}} = \frac{(3-\delta) \times (y-2\delta)^2}{\delta \times (1-y+2\delta)^2 \times P_{O_2}^{1/2}} \tag{41}$$

where K is the equilibrium constant of Reaction (35). Under a load condition, we have

$$i_{h^\bullet} = i_L + i_{V_O^{\bullet\bullet}} \tag{42}$$

The following P_{O_2} profile across the thickness L can be derived,

$$\frac{x}{L} = \frac{\int_{\ln Po_2(0)}^{\ln Po_2(x)} \frac{\sigma_{V_O^{\bullet\bullet}} \times (\sigma_{h^\bullet} - \sigma_L)}{\sigma_{h^\bullet} - \sigma_{V_O^{\bullet\bullet}} - \sigma_L} \times \mathrm{d}(\ln Po_2)}{\int_{\ln Po_2(0)}^{\ln Po_2(L)} \frac{\sigma_{V_O^{\bullet\bullet}} \times (\sigma_{h^\bullet} - \sigma_L)}{\sigma_{h^\bullet} - \sigma_{V_O^{\bullet\bullet}} - \sigma_L} \times \mathrm{d}(\ln Po_2)} \tag{43}$$

Fig. 6 shows the calculated P_{O_2} profiles across the LCC with a fuel mixture of CH_4 and H_2O (CH_4/H_2O = 2.5) [16]. The P_{O_2}-profile and electrical conductivity are dominated primarily by the low P_{O_2}. This phenomenon resembles the one shown in Fig. 2.

4.2. Electron-induced leakage current density

Fig. 7 shows the calculated $i_{V_O^{\bullet\bullet}} \cdot x$ vs. P_{O_2} across a 3 mm thick $La_{0.7}Ca_{0.3}CrO_3$ membrane exposed to air and fuel for four different temperatures. The uneven spacing of the profile is caused by the nonlinear relationship between δ and T. Since $i_{V_O^{\bullet\bullet}}$ is constant at any location in the LCC under steady state, $i_{V_O^{\bullet\bullet}} \cdot x$ is essentially proportional to x. P_{O_2} is linear with x up to ~90% of the total thickness, followed by a sharp increase just before reaching the air-side surface. The $i_{V_O^{\bullet\bullet}} \cdot x$ at which a sudden P_{O_2} change occurs increases with the temperature, indicating an increased ionic leakage current density.

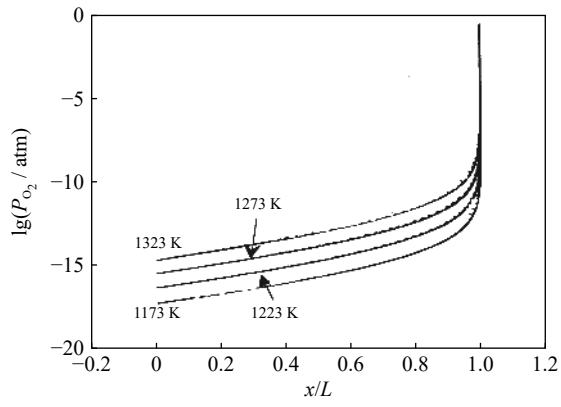

Fig. 6. Calculated transmembrane P_{O_2} profiles of $La_{0.7}Ca_{0.3}CrO_3$ at different temperatures. Adapted from I. Yasuda and M. Hishinuma, *J. Electrochem. Soc.*, vol. 143, 1583-1590 (1996) [16]. © IOP Publishing. Reproduced with permission. All rights reserved.

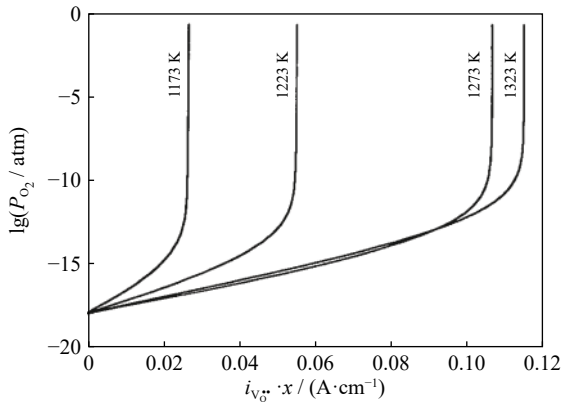

Fig. 7. Calculated P_{O_2} and ionic current density $i_{V_O^{\bullet\bullet}}$. The P_{O_2} at the fuel side is assumed to be 10^{-18} atm. Adapted from I. Yasuda and M. Hishinuma, *J. Electrochem. Soc.*, vol. 143, 1583-1590 (1996) [16]. © IOP Publishing. Reproduced with permission. All rights reserved.

Fig. 8 presents the variation of $i_{V_O^{\bullet\bullet}}$ with load current i_L. The negative value represents the current flowing from the air-side to the fuel-side of the interconnect, which corresponds to the operation of a SOFC. Under this SOFC mode, $i_{V_O^{\bullet\bullet}}$ decreases linearly with i_L. This is also understandable because the gradient of the electrochemical potential of oxide-ions increases as i_L decreases because the gradients of the chemical potential of oxygen and electrostatic potential are established in the opposite direction. Similar to the electron leakage in CeO_2-based electrolytes, increasing the i_L would lower ionic (oxygen vacancy) current density, implying that the load suppresses the loss of fuel due to this ionic leakage. Therefore, the most noticeable impact happens at low i_L,

where the SOFC's electrical efficiency is highest. Interestingly, under electrolysis mode (positive i_L), the increasing i_L would increase ionic leakage. However, transporting oxygen from the fuel to air through the IC would help the electrolysis process, such as H_2O splitting.

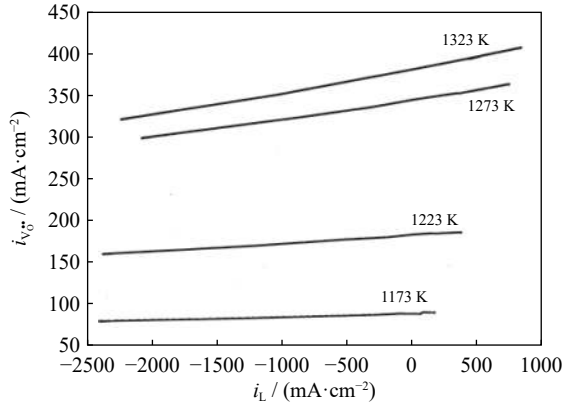

Fig. 8. Ionic current density vs. load-current density of a $La_{0.7}Cr_{0.3}O_3$ interconnect. Adapted from I. Yasuda and M. Hishinuma, *J. Electrochem. Soc.*, vol. 143, 1583-1590 (1996) [16]. © IOP Publishing. Reproduced with permission. All rights reserved.

5. Conclusion

The combination of the irreversible-thermodynamics-based transport of charged particles with the local "quasi-charge neutrality" principle has provided detailed information in oxygen partial pressure distribution across a solid oxide with either ionic or electronic dominated charge carrier, electronic/ionic leakage currents, and the effect of load current on the electrochemical leakage currents. The transport theory to an oxide-ion and electron-dominated mixed ion-electron conductor reveals that the lower oxygen partial pressure range primarily dominates the partial oxygen pressure distribution across a mixed conductor. The load current generally reduces leakage current. When these findings are applied to practical applications, they imply that leakage current may not be a serious problem for a device operating at high current but may be a problem in open-circuit or low-current conditions. Hence, minimizing the electrochemical leakage current of the electrolyte or ceramic interconnect is critical in maintaining the high electrical efficiency of solid oxide cells.

Acknowledgements

This material is based on the work supported by the U.S. Department of Energy's Office of Energy Efficiency and Renewable Energy through the Fuel Cell Technologies Office under award number DE-EE-0008842. We would also like to thank the National Science Foundation, United States for funding this study under award number 1801284.

Conflict of Interest

There is no conflict of interest.

References

[1] S.D. Ebbesen, S.H. Jensen, A. Hauch, and M.B. Mogensen, High temperature electrolysis in alkaline cells, solid proton conducting cells, and solid oxide cells, *Chem. Rev.*, 114(2014), No. 21, p. 10697.

[2] C.L. Wang, Y.C. Yu, J.J. Niu, Y.X. Liu, D. Bridges, X.Q. Liu, J. Pooran, Y.F. Zhang, and A.M. Hu, Recent progress of metal–air batteries—A mini review, *Appl. Sci.*, 9(2019), No. 14, art. No. 2787.

[3] Q.Y. Jiang, S. Faraji, D.A. Slade, and S.M. Stagg-Williams, A review of mixed ionic and electronic conducting ceramic membranes as oxygen sources for high-temperature reactors, *Membr. Sci. Technol.*, 14(2011), p. 235.

[4] L. Heyne, Electrochemistry of mixed ionic-electronic conductors, [in] S. Geller, ed., *Solid Electrolytes*, Springer-Verlag Berlin Heidelberg, New York, 1977, p. 169..

[5] C. Wagner, Beitrag zur theorie des anlaufvorgangs, *Z. Phys. Chem.*, 21B(1933), No. 1, p. 25.

[6] S.R. De Groot, *Thermodynamics of Irreversible Processes*, North-Holland Publication Company, Amsterdam, 1951.

[7] H. Rickert, *Electrochemistry of Solids—An Introduction*, Springer-Verlag Berlin Heidelberg, New York, 1982, p. 79.

[8] J. Maier, *Physical Chemistry of Ionic Materials: Ions and Electrons in Solids*, John Wiley & Sons Ltd, Chichester, 2004, p. 294.

[9] G.E. Murch, The haven ratio in fast ionic conductors, *Solid State Ionics*, 7(1982), No. 3, p. 177.

[10] N.S. Choudhury and J.W. Patterson, Performance characteristics of solid electrolytes under steady-state conditions, *J. Electrochem. Soc.*, 118(1971), No. 9, art. No. 1398.

[11] I. Riess, Current–voltage relation and charge distribution in mixed ionic electronic solid conductors, *J. Phys. Chem. Solids*, 47(1986), No. 2, p. 129.

[12] A. Mineshige, T. Yasui, N. Ohmura, M. Kobune, S. Fujii, M. Inaba, and Z. Ogumi, Oxygen chemical potential and mixed conduction in doped ceria under influence of oxygen partial pressure gradient, *Solid State Ionics*, 152-153(2002), p. 493.

[13] B.C.H. Steele, Appraisal of $Ce_{1-y}Gd_yO_{2-y/2}$ electrolytes for IT-SOFC operation at 500°C, *Solid State Ionics*, 129(2000), No. 1-4, p. 95.

[14] B. Dalslet, P. Blennow, P.V. Hendriksen, N. Bonanos, D. Lybye, and M. Mogensen, Assessment of doped ceria as electrolyte, *J. Solid State Electrochem.*, 10(2006), No. 8, p. 547.

[15] I. Yasuda and T. Hikita, Electrical conductivity and defect structure of calcium-doped lanthanum chromites, *J. Electrochem. Soc.*, 140(1993), No. 6, p. 1699.

[16] I. Yasuda and M. Hishinuma, Electrochemical properties of doped lanthanum chromites as interconnectors for solid oxide fuel cells, *J. Electrochem. Soc.*, 143(1996), No. 5, p. 1583.